

Adaptation Dynamics in Densely Clustered Chemoreceptors

William Pontius^{1,2}, Michael W. Sneddon^{2,3✉}, Thierry Emonet^{1,2*}

1 Department of Physics, Yale University, New Haven, Connecticut, United States of America, **2** Department of Molecular, Cellular, and Developmental Biology, Yale University, New Haven, Connecticut, United States of America, **3** Interdepartmental Program in Computational Biology and Bioinformatics, Yale University, New Haven, Connecticut, United States of America

Abstract

In many sensory systems, transmembrane receptors are spatially organized in large clusters. Such arrangement may facilitate signal amplification and the integration of multiple stimuli. However, this organization likely also affects the kinetics of signaling since the cytoplasmic enzymes that modulate the activity of the receptors must localize to the cluster prior to receptor modification. Here we examine how these spatial considerations shape signaling dynamics at rest and in response to stimuli. As a model system, we use the chemotaxis pathway of *Escherichia coli*, a canonical system for the study of how organisms sense, respond, and adapt to environmental stimuli. In bacterial chemotaxis, adaptation is mediated by two enzymes that localize to the clustered receptors and modulate their activity through methylation-demethylation. Using a novel stochastic simulation, we show that distributive receptor methylation is necessary for successful adaptation to stimulus and also leads to large fluctuations in receptor activity in the steady state. These fluctuations arise from noise in the number of localized enzymes combined with saturated modification kinetics between the localized enzymes and the receptor substrate. An analytical model explains how saturated enzyme kinetics and large fluctuations can coexist with an adapted state robust to variation in the expression levels of the pathway constituents, a key requirement to ensure the functionality of individual cells within a population. This contrasts with the well-mixed covalent modification system studied by Goldbeter and Koshland in which mean activity becomes ultrasensitive to protein abundances when the enzymes operate at saturation. Large fluctuations in receptor activity have been quantified experimentally and may benefit the cell by enhancing its ability to explore empty environments and track shallow nutrient gradients. Here we clarify the mechanistic relationship of these large fluctuations to well-studied aspects of the chemotaxis system, precise adaptation and functional robustness.

Citation: Pontius W, Sneddon MW, Emonet T (2013) Adaptation Dynamics in Densely Clustered Chemoreceptors. PLoS Comput Biol 9(9): e1003230. doi:10.1371/journal.pcbi.1003230

Editor: Christopher V. Rao, University of Illinois at Urbana-Champaign, United States of America

Received: May 1, 2013; **Accepted:** August 3, 2013; **Published:** September 19, 2013

Copyright: © 2013 Pontius et al. This is an open-access article distributed under the terms of the Creative Commons Attribution License, which permits unrestricted use, distribution, and reproduction in any medium, provided the original author and source are credited.

Funding: This work was supported by the James McDonnell Foundation, the Paul G. Allen Family Foundation, and the National Institute of Health. The funders had no role in study design, data collection and analysis, decision to publish, or preparation of the manuscript.

Competing Interests: The authors have declared that no competing interests exist.

* E-mail: thierry.emonet@yale.edu

✉ Current address: Physical Biosciences Division, Lawrence Berkeley National Lab, Berkeley, California, United States of America.

Introduction

High-resolution microscopy has revealed the exquisite spatial organization of signaling pathways and their molecular constituents. Understanding the computations performed by biological networks therefore requires taking the spatiotemporal organization of the reactants into account [1]. One feature common to many signal transduction pathways is the clustering of receptors in the cell membrane. This arrangement has been observed for diverse receptor types [2] such as bacterial chemoreceptors [3–6], epidermal growth factor receptors [7], and T cell antigen receptors [8]. Receptor clustering provides a mechanism for controlling the sensitivity [9,10] and accuracy [11,12] of a signaling pathway. Moreover, by controlling which types of receptors participate in clusters a cell can achieve spatiotemporal control over the specificity of the signaling complexes.

While clustering receptors can tune the sensitivity and specificity of a signaling pathway, organizing receptors into clusters also imposes novel constraints on the kinetics of the pathway. Temporal modulations of the activity of signaling complexes,

such as adaptation, are typically achieved via posttranslational modification of the cytoplasmic tail of the receptors by various enzymes. The localization of the receptor substrate into clusters implies that trafficking of enzymes between the cytoplasm and the cluster and between receptors within a cluster is likely to be an important determinant of the dynamics of such modulations. Recent theoretical studies of the effect of the localization of enzymes and substrates on signaling kinetics have shown that spatiotemporal correlations between reactants can significantly affect the signaling properties of these pathways [13–15].

One well-characterized system in which the spatial organization of receptors plays a significant role is the chemotaxis system of the bacterium *Escherichia coli* [16–18]. *E. coli* moves by performing a random walk alternating relatively straight runs with sudden changes of direction called tumbles. The probability to tumble is modulated by a two-component system in which transmembrane receptors regulate the activity of a histidine kinase CheA, which in turn phosphorylates the response regulator CheY. Phosphorylated CheY rapidly diffuses through the cell and binds the flagellar motors to induce tumbling. The tumbling rate decreases in

Author Summary

To navigate their environments, organisms must remain sensitive to small changes in their surroundings while adapting to persistent conditions. Bacteria travel by performing a random walk biased toward nutrients and away from toxins. The decision of a bacterium to continue in a given direction or to reorient is controlled by the state of its chemoreceptors. Chemoreceptors assemble into large polar clusters, an arrangement required for the amplification of small stimuli. We investigate how this organization affects the kinetics of the enzymatic reactions through which the receptors adapt to persistent stimuli. We show that clustering can lead to large fluctuations in the state of the receptors, which have been observed in *Escherichia coli* and may aid in the navigation of weak stimulus gradients and the exploration of sparse environments. Additionally, we show that these fluctuations can occur around a mean receptor state robust to changes in the numbers of the adaptation enzymes. Since enzyme expression levels vary across a population, this feature ensures a high proportion of functional cells. Our study clarifies the relation between fluctuations, adaptation, and robustness in bacterial chemotaxis and may inform the study of other biological systems with clustered receptors or similar enzyme-substrate interactions.

response to chemical attractants and increases in response to repellants, allowing the bacterium to navigate its environment.

Chemoreceptor clustering affects both signal amplification and adaptation to persistent stimuli, which together enable bacteria to remain sensitive to over five orders of magnitude of ligand concentration [19]. Signal amplification arises from allosteric interactions between clustered receptors [9,20–23] whereas adaptation is mediated by the activity of two enzymes: CheR methylates inactive receptors, thereby reactivating them, while CheB demethylates active receptors, deactivating them. This arrangement implements an integral feedback mechanism [24], enabling kinase activity and therefore cell behavior to return to approximately the same stationary point following response to stimulus [25,26]. The localization of enzymes to the cluster is facilitated by a high-affinity tether site present on most receptors. This tether, together with the dense organization of the cluster, enables localized enzymes to modify multiple receptors within a range known as an assistance neighborhood [27]. Modeling efforts have shown that assistance neighborhoods are required for precise adaptation when receptors are strongly coupled [28].

Precise adaptation, however, is not by itself sufficient for successful chemotaxis. The dynamics of the adaptation process, including the rate of receptor modification and the level of spontaneous fluctuation in receptor activity, are also critical determinants of chemotactic performance [29–35]. Recent measurements of the dynamic localization of chemotaxis proteins have shown that the time scale of CheR and CheB localization to the receptor cluster is comparable to the time scale of adaptation [36] and therefore expected to affect the dynamics significantly. Moreover, dense clustering may enable localized enzymes to perform a random walk over the receptor lattice without returning to the cytoplasmic bulk, a proposed process termed brachiation [37] that may lead to more efficient receptor modification.

Here we analyze how the spatiotemporal localization of the adaptation enzymes to the receptor cluster affects the dynamics of the adaptation process. First we build a stochastic simulation of the chemotaxis system taking into account the organization of the receptors into large clusters [4,6], the slow exchange of enzymes

between the cytoplasm and the clusters [36], enzyme brachiation [37], and assistance neighborhoods [27,28,38]. This model quantitatively recapitulates experimental observations of the magnitude of the spontaneous fluctuations in single cells [39–42] and the kinetics of adaptation averaged over multiple cells [43]. Notably, while localized enzymes in this model operate at saturation, the output of the system nonetheless remains robust to cell-to-cell variation in enzyme expression levels [44], in contrast to the covalent modification system studied by Goldbeter and Koshland [12]. We therefore resolve the question of how large spontaneous fluctuations might coexist with a robust mean output in the system [30]. We interpret these results in the second part of the paper, using a mean-field analytical model to examine the molecular mechanisms underlying these features and their relation to receptor clustering.

Results

Numerical model of adaptation dynamics in a chemoreceptor cluster

We used the rule-based simulation tool NFsim [45] to create a stochastic model of the bacterial chemotaxis system that accounts for the organization of chemoreceptors into a large, dense, hexagonal lattice [4]. Like the Gillespie algorithm, NFsim computes exact stochastic trajectories, but avoids the full enumeration of the reaction network, which can undergo combinatorial explosion, by using rules to generate reaction events [45]. In the simulation, each chemoreceptor dimer is represented by an object with one tether site, one modification site, and a methylation level ranging from 0 to 8. We model a single contiguous lattice consisting typically of 7200 dimers, although we consider different sizes as well. The structure of the lattice is fully specified by enumerating for each dimer its six nearest neighboring dimers. Receptor cooperativity is modeled using Monod-Wyman-Changeux (MWC) complexes consisting of six receptor dimers (Fig. 1A). The activity a of each signaling complex depends on the methylation and ligand-binding state of the dimers in the complex and is calculated from Eq. (13) (Methods) as previously described [23,28]. The implementation of this model in NFsim is discussed in the Supporting Text S1.

Receptor modification occurs through the enzymes CheR and CheB, which are each modeled as having two binding sites, one specific to the receptor tether and one specific to the modification site. In the model, CheR and CheB dynamically bind and unbind both of these sites. CheR participates in the reactions illustrated in Fig. 1B. The possible states of the enzyme are: free and dispersed in the cytoplasmic bulk, or bound to one or both of the tether and modification sites. Enzymes in the bulk localize to the cluster by binding either the tether site or the modification site directly. The time scales of these binding reactions (Fig. 1B, blue arrows) are the slowest in the present model: ~ 15 s for localization through tether binding, as measured [36], and longer for modification site binding, reflecting the lower affinity of enzymes for the modification site. Once bound to the tether or modification site, an enzyme may bind the modification site or tether, respectively, of the receptor to which it is already bound (Fig. 1B, red arrows) or any of its six nearest neighbors (green arrows). Therefore the assistance neighborhood consists of seven dimers, consistent with measurements [27]. Assistance neighborhoods are unique for each receptor dimer and therefore overlap. Accordingly, in the simulation individual receptor dimers participate in multiple assistance neighborhoods. Since these reactions are confined to small volumes (given by the ~ 5 nm tether radius [46]), they proceed at high rates (1–10 ms time scales; see Text S1). The

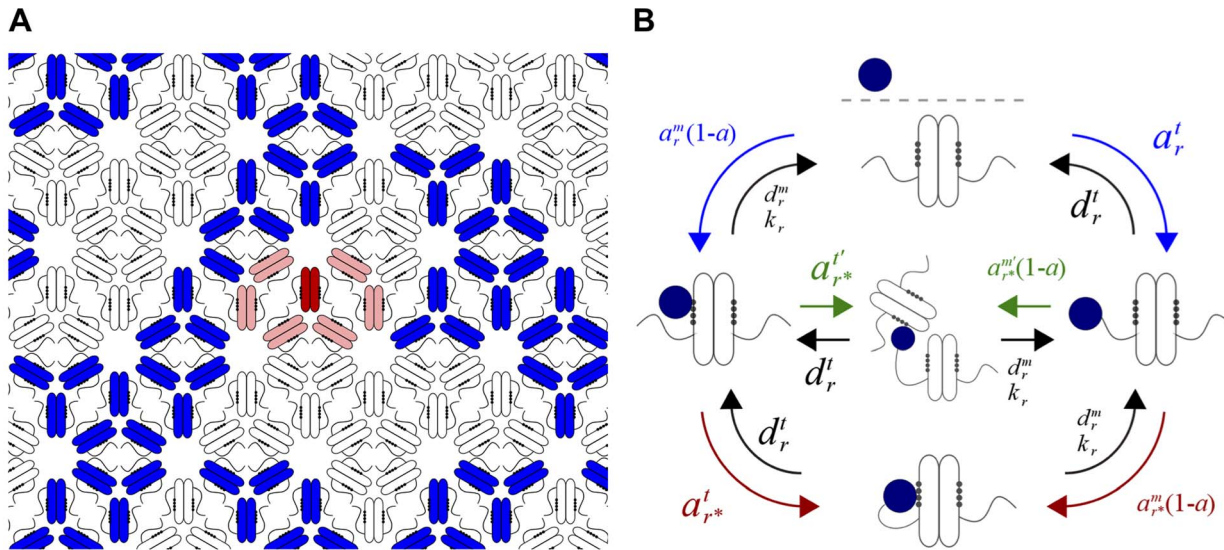


Figure 1. Adaptation reactions on the chemoreceptor lattice. (A) Bacterial chemoreceptors assemble into trimers of dimers that organize to form a dense hexagonal lattice. Most chemoreceptors have tether and modification sites. In the model, the assistance neighborhood for a given receptor (red) consists of all the receptors accessible by its tether, here taken to be the six nearest dimers (light red) in addition to itself. Groups of six receptor dimers switch cooperatively between active (blue) and inactive (white) states according to a MWC model. (B) Modeled reactions between CheR and the chemoreceptors with corresponding rates. Binding rates to the modification site depend on the receptor activity a . CheR in the cytoplasmic bulk may bind either the tether or modification site of a receptor (blue arrows, rates a_r^t and $a_r^m(1-a)$ respectively). Once bound to the tether or modification site it may respectively bind the modification site or tether of itself (red arrows, rates $a_{r^*}^m(1-a)$ and $a_{r^*}^t$ respectively) or any other receptor within its assistance neighborhood (green arrows, rate $a_{r^*}^m(1-a)$) to bind the neighboring modification site and rate $a_{r^*}^t$ to bind the neighboring tether). Black arrows denote unbinding and catalytic steps (catalytic rate k_r ; tether unbinding rate d_r^t ; modification site unbinding rate d_r^m). CheB-P participates in analogous reactions. In the rates, superscripts m and t denote binding to the modification site and tether site, respectively. The subscripts r and b denote CheR and CheB reactions, respectively. doi:10.1371/journal.pcbi.1003230.g001

activity-dependent binding rate of CheR to the modification site is proportional to $1 - a$, while the rates of all other CheR reactions are taken to be independent of activity. Phosphorylated CheB (CheB-P) participates in completely analogous reactions except that the rate of binding the modification site is proportional to a . CheB phosphorylation proceeds at a rate proportional to the activity of the receptor cluster (Text S1). For simplicity we assume that only CheB-P can localize to the receptor cluster since its affinity for the tether is much higher than that of CheB [47].

Our study is the first to incorporate enzyme brachiation [37], assistance neighborhoods [28,38], cooperative amplification of the input signal [9,22,23], activity-dependent adaptation kinetics [25], and a large contiguous receptor cluster into a single model. This model specifically extends two earlier models. The first of these models considered enzyme brachiation on a large receptor cluster [37], but did not include activity-dependent kinetics, receptor cooperativity, or any modification of the receptors. The second of these models included activity-dependent kinetics, cooperativity, and assistance neighborhoods [28,38] but excluded enzyme brachiation and limited the system size to a single MWC complex consisting of 19 dimers. Here we take advantage of the flexibility and efficiency of NFsim to examine how all of these processes together determine the dynamics of adaptation.

Calibration of the model parameters is discussed in the Supporting Text S1. Supporting Tables S1 and S2 present the full set of simulation parameters. We note that our model includes only Tar receptors. This choice enabled us to compare our model directly to measurements of the adaptation kinetics [43] performed on cells lacking receptors other than Tar. These measurements were obtained by exposing cells to time-dependent exponential ramps of methyl-aspartate, a protocol that we modeled *in silico*

(Fig. 2A and Fig. S2) to verify the calibration of the kinetics of our model. In the remainder of the paper we denote this calibrated model as the reference model **M1**.

Distributive methylation leads to precise adaptation

Together with the dense organization of the receptor lattice, the presence of the tether site on each receptor gives rise to assistance neighborhoods [27] and possibly enzyme brachiation [37]. During the brachiation process, enzymes successively bind and unbind the tethers and modification sites on different, neighboring receptors, enabling them to perform a random walk over the lattice without returning to the bulk. Both assistance neighborhoods and enzyme brachiation should increase the distributivity of the methylation process, meaning that sequential (de)methylation events catalyzed by a single enzyme will tend to take place on different receptors. In a distributive scheme, therefore, an enzyme will tend to modify multiple receptors during its residence time on the cluster. Moreover, it will tend to methylate receptors in an even fashion, rather than sequentially modifying a single receptor until it is fully (de)methylated. Since brachiation enables some randomization of enzyme position between methylation events, it should lead to a more distributive methylation process.

To investigate how distributivity affects adaptation we compared our reference model **M1**, which includes assistance neighborhoods and brachiation, to a model in which the binding of tethered enzymes to the modification sites of neighboring receptors (and modification site-bound enzymes to neighboring tethers) is not allowed, denoted **M2** (Table 1). Disabling these reactions both removes assistance neighborhoods and prevents enzyme brachiation. As a result, methylation is more processive. In this scheme, an enzyme remains bound to and modifies only a

Table 1. Summary of numerical models.

Numerical model	Features
M1	Reference model; assistance neighborhoods and enzyme brachiation; activity-dependent binding kinetics; MWC receptor cooperativity.
M2	Derived from M1 ; no assistance neighborhoods or enzyme brachiation.
M3	Derived from M1 ; less efficient brachiation relative to M1 .
B1	No enzyme tethering or lattice structure; activity-dependent binding kinetics; MWC receptor cooperativity.
B2	Derived from B1 by increasing enzyme-receptor affinities.

doi:10.1371/journal.pcbi.1003230.t001

single receptor during its residence time in the cluster. This scheme increases the probability that CheR and CheB will become bound to receptors with high or low methylation levels, respectively. Consequently, enzymes will tend to have low affinity for their local modification sites and modification will proceed in an inefficient manner compared to a distributive scheme. In **M2**, adaptation to both small (5 μM) and large (1 mM) steps of the attractant methyl-aspartate becomes much slower (Fig. 2B, light gray) than in the reference model **M1** (Fig. 2B, black). Precise adaptation is also severely compromised for the large stimulus.

We also consider the case in which enzyme brachiation is made less efficient, but adaptational assistance is not eliminated. To examine this intermediate model (**M3**), we decreased the unbinding rates from the tether $d'_{r,b}$ relative to **M1**. As a result, more methylation events occur before an enzyme moves on the lattice. This leads to less efficient brachiation than in **M1** but preserves assistance neighborhoods. As a result, adaptation to the large stimulus is less precise compared to **M1** but more precise than **M2** (Fig. 2B).

The picture that emerges is that the distributivity of the modification process is an important determinant of the precision of adaptation. Adaptational assistance and enzyme brachiation increase the distributivity of modification and lead to more precise adaptation in our model of the full receptor lattice. This result extends previous findings that the ability of tethered CheR and CheB to modify several receptors within an assistance neighborhood is necessary for precise adaptation within a single MWC complex [28,38]. In our simulations, as in these previous studies, increasing the distributivity of receptor methylation reduces the time CheR and CheB spend bound to highly methylated and demethylated receptors, respectively. Consequently, the methylation rate in distributive models is largely independent of the methylation levels of individual receptors, resulting in more precise adaptation. Additionally, (de)methylation rates are higher than in the more processive schemes because the enzymes spend less time interacting with receptors that are already highly methylated or demethylated. Indeed, plotting the rate of methylation after the step stimulus for the three simulations depicted in Fig. 2B (bottom panel) indicates that it is highest in the most distributive model **M1** (Fig. S7 and Text S1).

Distributive methylation leads to large steady-state fluctuations

Experiments and modeling efforts strongly suggest that the adaptation mechanism of the bacterial chemotaxis system introduces slow spontaneous fluctuations in the activity of the receptor-kinase complex with a standard deviation of $\sim 5\text{--}10\%$ of the mean [33,39–42,48,49]. These fluctuations are thought to lead to long-tailed distributions of run durations [39,50] and may

enhance navigation in shallow gradients and exploration [30,32,33,35,39]. Since distributivity affects the kinetics of adaptation, it is also likely to affect the spontaneous fluctuations of the system. Fig. 2C compares the level of fluctuation in receptor activity about the unstimulated steady-state level for each model at different expression levels of CheR. The model **M1** exhibits fluctuations of the same order as those measured experimentally, particularly at low CheR levels for which the standard deviation σ_a of fluctuations exceeds 7% of the mean activity a_0 . Notably, the magnitude of this noise is reduced when receptor modification is made less distributive in models **M2** and **M3**. These results suggest that the features required for successful adaptation, assistance neighborhoods and brachiation, also lead to experimentally observed levels of signaling noise. The mechanism underlying these relations will be discussed in a later section with insights provided by an analytical model.

Cells within an isogenic wild-type population are known to exhibit significant cell-to-cell variability in the level of signaling noise [33,39–41]. To what extent does this variability arise from cell-to-cell variability in the expression levels of the chemotaxis proteins? Our simulations of the model **M1** indicate that the level of signaling noise is sensitive to the relative amounts of CheR and CheB in the cell (Fig. 2C). However, the multicistronic organization of *cheR* and *cheB* on the chromosome ensures that the ratio of CheR to CheB is approximately conserved in each cell within a wild-type population due to cotranscription [44,51]. Therefore variability in signaling noise levels must arise largely from correlated variation in the expression levels of the chemotaxis proteins. Using our stochastic simulation of enzyme dynamics on the receptor lattice (**M1**), we investigated the effects of covarying the number of CheR, CheB and chemoreceptors. We sampled cells from across a population in which CheR, CheB and chemoreceptor counts all vary according to a log-normal distribution (Fig. S5) obtained from measurements of CheY-YFP levels expressed from the native chromosomal locus [44]. Mean protein expression levels were set according to immunoblotting measurements [52]. To study only the effects of concerted variation in protein levels, we ignored intrinsic noise, thereby preserving the ratio of CheR/CheB/receptors. We found that the level of signaling noise varies widely between each sampled cell, between 3 and 10% of the mean (Fig. 3A). This degree of variation in signaling noise levels agrees well with measurements performed across a wild-type population [40,41]. Additionally, we found that cells with low expression levels of the chemotaxis proteins are predicted to exhibit the large fluctuations, $\sim 10\%$ of the mean level. Consequently, we expect cells with high levels of signaling noise to be present even in populations across which the CheR to CheB ratio is maintained at the single cell level.

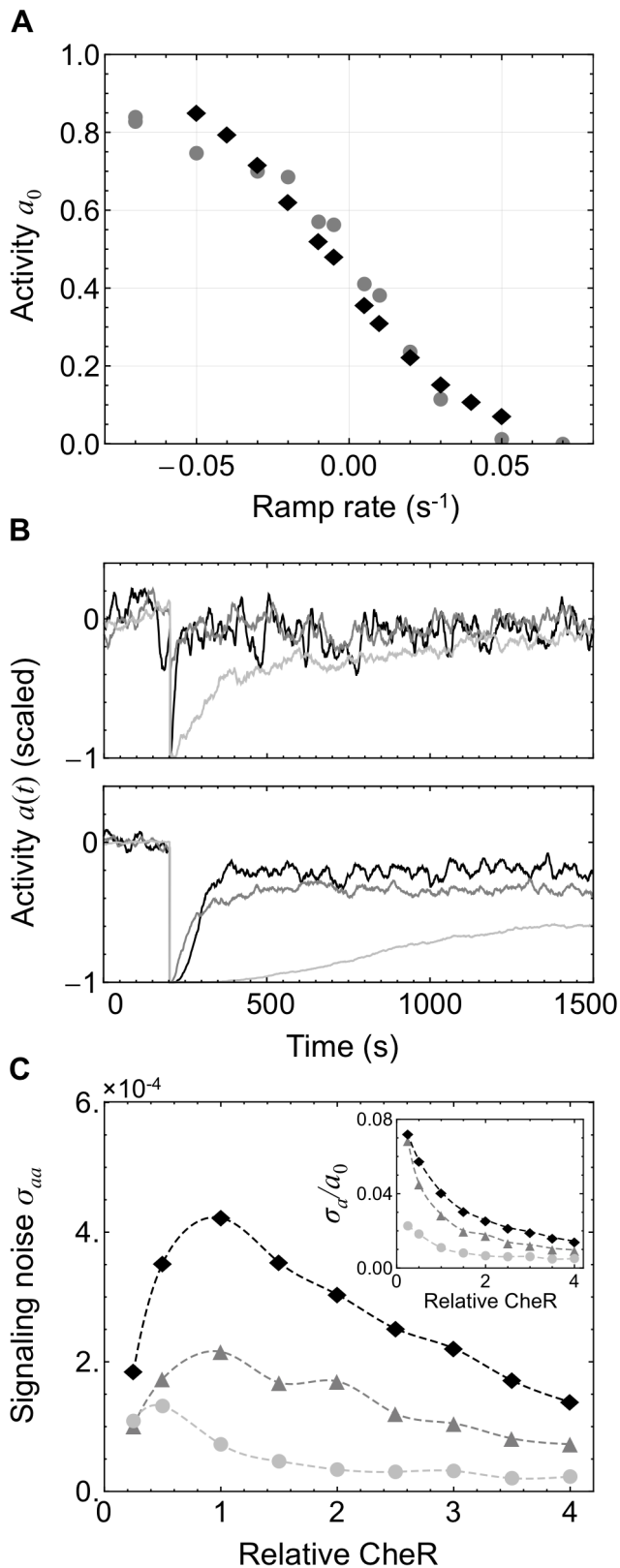


Figure 2. Processive receptor methylation compromises adaptation and decreases signaling noise. Compared are three simulated models of the chemotaxis adaptation system: **M1** with assistance neighborhoods and efficient brachiation (black traces), **M2** with no assistance neighborhoods or brachiation (light gray), and **M3** with assistance neighborhoods but inefficient brachiation (dark gray).

Methylation is more processive in **M2** and **M3** than in **M1**. As processivity increases, enzymes become more localized to receptors that are already highly methylated (CheR) or demethylated (CheB), limiting their effectiveness. (A) The kinetics of **M1** were calibrated by comparison to population-level measurements (gray) [43]. The model was exposed to simulated time-varying exponential ramps of methyl-aspartate and the resulting steady-state activity a_0 recorded (black). (B) Response to small (5 μ M) and large (1 mM) MeAsp step stimulus at applied at $t=200$ s as measured by receptor activity $a(t)$. While all models adapt to the small stimulus (top), they fail to adapt precisely to the large stimulus (bottom). For the large stimulus, higher processivity leads to less precise adaptation with **M1** performing best and **M2** worst. Activities have been scaled and recentered with steady-state values at 0. (C) Increasing processivity also decreases the magnitude of fluctuations in $a(t)$ in the adapted state around the mean value a_0 . Plotted is the variance σ_{aa} of $a(t)$ and the noise relative to the mean output σ_{aa}/a_0 (inset) for different expression levels of the enzyme CheR. Fluctuations are largest in **M1** and smallest in model **M2**. doi:10.1371/journal.pcbi.1003230.g002

High levels of signaling noise occur around a robust adapted level

In previous models of the chemotaxis system in which enzyme localization is not considered, the slow, spontaneous fluctuations in the activity of the system were traced back to the ultrasensitive nature of the methylation and demethylation reactions, which were assumed to operate near saturation [30]. This mechanism, however, is insufficient to explain the large magnitude of the noise observed experimentally in individual cells. Indeed, using a stochastic simulation of a recent representative analytical model (Model **B1**) in which the authors calibrated the rates of methylation-demethylation using direct measurements of the average response of the receptor activity to ramps of attractant [43], we observe at most 2–3% relative noise for the individual cell (Fig. 3B). The model **B1** incorporates activity-dependent binding of the enzymes to the modification sites, but does not consider any aspects of enzyme localization via tether binding (Table 1). Additionally, while this model includes cooperative receptor-receptor interactions using a MWC model, given by Eq. (13) as for **M1**, it considers neither the geometry of the receptor cluster nor the resulting features of adaptational assistance and enzyme brachiation. Higher noise levels can be obtained in this model by increasing the enzyme-substrate affinities tenfold (Model **B2**). These higher affinities, however, result in a steady-state activity that is ultrasensitive to total enzyme counts (Fig. 3C, light gray). In this case the addition or subtraction of only a few adaptation enzymes in the cell is sufficient to switch the system between the fully active and fully inactive states. This scenario is biologically unacceptable since small fluctuations in gene expression across a population would lead to large numbers of non-functional cells with either fully active or inactive receptors at steady state. Parameter values for models **B1** and **B2** are given in Tables S4 and S6.

Interestingly, in our model accounting for the localization of enzymes to the receptor cluster, large fluctuations around the steady state activity are present even though the mean activity remains relatively robust to changes in enzyme counts. Fig. 3B shows the dependence of the steady-state fluctuations in **M1** on total CheR count with all other parameters fixed. **M1** exhibits activity fluctuations that exceed 7% of the mean value a_0 for low CheR counts and are significantly larger than those of the model **B1** for all CheR values. While the noise level is high, the mean receptor activity at steady state, a_0 , is only modestly sensitive to changes in the total CheR count (Fig. 3C, black). The specific features enabling the coexistence of large fluctuations with a robust

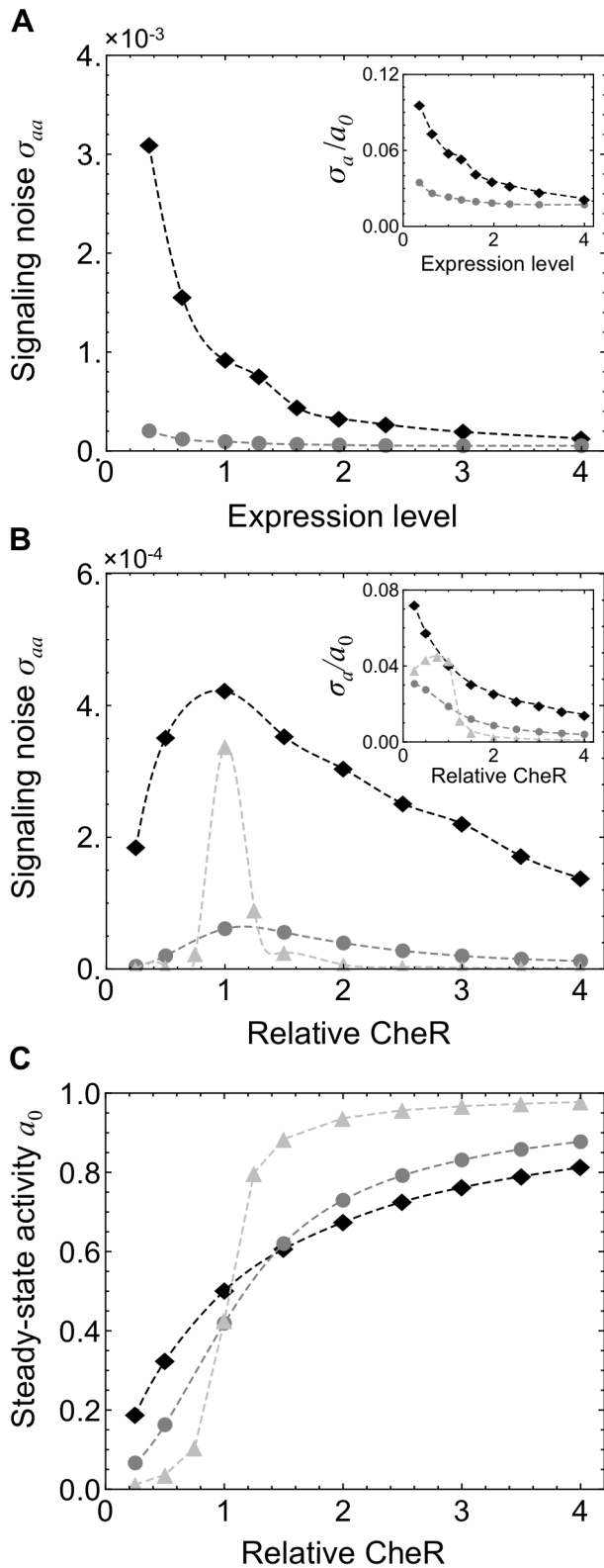


Figure 3. Spontaneous output of the bacterial chemotaxis system. Results are from stochastic simulations of a chemotaxis model **M1** with a hexagonal receptor lattice and explicit enzyme tethering and the model **B1** with no tethering or lattice structure. (A) We sampled representative cells from a population in which the ratio CheR/CheB/chemoreceptors is maintained but the overall expression level varies. Stochastic simulation of model **M1** (black) predicts that some cells in

this population will exhibit especially large fluctuations $\sigma_a/a_0 \sim 10\%$. The magnitude of fluctuations increases sharply as the level of protein expression decreases. Noise levels in **M1** are significantly larger than in **B1** (gray) at all expression levels. The horizontal axis is normalized by the most common expression level. (B) The variance σ_{aa} of fluctuations in receptor activity is shown as CheR is varied while all other proteins are expressed at their mean levels. The variance σ_{aa} is significantly greater in **M1** (black, diamonds) than in **B1** (gray, circles). The model **M1** produces exceeding 7% of the mean level (black, inset), while noise in **B1** remains less than $\sim 3\%$ (gray, inset). The noise was increased in **B2** by increasing the enzyme-receptor affinities tenfold (light gray) relative to **B1**. (C) **M1** and the (black, diamonds) and **B1** (gray, circles) also exhibit similar dependence of the mean receptor activity at steady state a_0 on CheR count. The model **B2** with higher enzyme-receptor affinities exhibits highly ultrasensitive dependence on the CheR count (light gray).

doi:10.1371/journal.pcbi.1003230.g003

steady state are discussed in a later section with reference to an analytical model.

Finally, we compare the noise levels predicted by the models **M1** and **B1** across a cell population. When cell-to-cell variability in receptor and enzyme counts is taken into account we observe that **B1**, which does not account for receptor clustering or enzyme localization, exhibits insufficiently large fluctuations ($\sigma_a/a_0 < 4\%$) across the entirety of the population (Fig. 3A). In contrast, **M1** exhibits levels of noise similar to those measured experimentally [33,40,41], as discussed in the previous section.

Mean-field model with distributive receptor methylation and precise adaptation

To investigate the mechanisms underlying our numerical results, we constructed an approximate model that can be solved analytically. Here we provide a mathematical derivation of the model. Analysis of the adaptation mechanism using this model is provided in the next section.

At the heart of this model is a covalent modification scheme that describes the kinetics of receptor methylation by CheR and CheB, similar in form to previous models [12,25,30,53,54]. In order to modify the receptors, however, we require that CheR and CheB be localized to the receptor cluster by being bound to the tether site. In this treatment, CheR may exist in three states: free and dispersed in the cytoplasmic bulk (R), bound only to the tethering site of a receptor (R^*), and bound to both the tether site and modification site of receptors ($\overline{R^*T}$). The notation for the states ($B_p, B_p^*, \overline{B_p^*T}$) of phosphorylated CheB is analogous. Unphosphorylated CheB is assumed not to interact with the receptors and therefore only exists in the bulk (B). For simplicity, we assume that enzymes in the bulk always bind the higher-affinity tether sites on the receptors prior to binding the modification sites. Since the model includes reactions occurring in multiple volumes and will later be used for stochastic calculations, all molecular species below are quantified by number rather than concentration. Therefore, the binding rates as written implicitly include a factor of the inverse of the reaction volume. In the model, active receptor complexes phosphorylate CheB at a rate a_p and CheB autodephosphorylates at rate d_p , leading to $dB_p/dt = a_p T_{Tot} a B - d_p B_p$, which we take to be in the steady state, yielding $B_p = a_p T_{Tot} a B / d_p$. We assume that only bulk CheB (B, B_p) participates in the phosphorylation reactions.

Defining $R_{Tot}^* = R^* + \overline{R^*T}$ and $B_{p,Tot}^* = B_p^* + \overline{B_p^*T}$ as the total number of tether-bound CheR and CheB-P, the dynamics of enzymes in the bulk binding to the tether site is modeled by

$$\frac{d}{dt} R_{Tot}^* = a_r^l T_{Tot} R - d_r^l R^* \quad (1)$$

$$\frac{d}{dt} B_{p, Tot}^* = a_b^l T_{Tot} B_p - d_b^l B_p^* \quad (2)$$

Here (a_r^l, a_b^l) denote the rates of cytoplasmic enzymes binding the tether site and (d_r^l, d_b^l) denote the rates of enzymes bound only to the tether unbinding the tether and dispersing into the bulk. Since the number of tether sites greatly exceeds the number of CheR and CheB [52], we assume it to be constant and equal to the total number of receptors T_{Tot} . Enzymes bound to the tether may bind the modification site according to

$$\frac{d}{dt} \overline{R^* T} = a_{r^*}^m (1-a) R^* - (d_r^m + k_r) \overline{R^* T} \quad (3)$$

$$\frac{d}{dt} \overline{B_p^* T} = a_{b^*}^m a B_p^* - (d_b^m + k_b) \overline{B_p^* T}, \quad (4)$$

in which $(a_{r^*}^m, a_{b^*}^m)$ are the rates of a tether-bound enzyme to bind the receptor modification site, (d_r^m, d_b^m) are the unbinding rates from the modification site, and (k_r, k_b) are catalytic rates for demethylation and methylation of the modification site, respectively. Binding to the modification site is dependent on the activity of the receptor. Eqs. (3, 4) employ a mean-field approximation by assuming that the activity of the receptor whose modification site is to be bound is equal to the mean activity of all receptors in the cell, a . This assumption makes the methylation process in this model fully distributive. Therefore the mean-field model represents the limit of a single, maximally large assistance neighborhood, encompassing all receptors, or infinitely fast brachiation, in which enzymes completely randomize their position on the lattice between methylation events. Relaxing this assumption requires a more detailed analytical model, which is explored in the Supporting Text S1.

Since Eqs. (3, 4) describe a binding reaction confined to the ~ 5 nm radius defined by the tether [46], the kinetics are fast relative to other reactions in the model (Text S1). We take $d\overline{R^* T}/dt = d\overline{B_p^* T}/dt = 0$, leading to an expression for the number of enzymes bound to both tethers and modification sites

$$\overline{R^* T} = \frac{a_{r^*}^m}{d_r^m + k_r} (1-a) R^* \equiv \frac{1-a}{K_r} R^* \quad (5)$$

$$\overline{B_p^* T} = \frac{a_{b^*}^m}{d_b^m + k_b} a B_p^* \equiv \frac{a}{K_b} B_p^* \quad (6)$$

Here K_r and K_b are dimensionless constants analogous to Michaelis-Menten constants. The rate of change of the *total* methylation level M of all MWC complexes in the system (the total number of methylated receptor sites across all receptors in the cell) is

$$\frac{dM}{dt} = k_r \overline{R^* T} - k_b \overline{B_p^* T} = \frac{k_r}{K_r} (1-a) R^* - \frac{k_b}{K_b} a B_p^* \quad (7)$$

Using Eqs. (5–7), we write the equation describing changes in average methylation level per $2N$ -receptor MWC complex, $m = M(2N/T_{Tot})$, in the form familiar from the Goldbeter-Koshland system [12,30,54]

$$\frac{dm}{dt} = \frac{2N}{T_{Tot}} \left[\frac{k_r R_{Tot}^* (1-a)}{K_r + 1-a} - \frac{k_b B_{p, Tot}^* a}{K_b + a} \right] + \eta_m \quad (8)$$

The tether-binding reactions Eqs. (1, 2) may be rewritten in terms of R_{Tot}^* and $B_{p, Tot}^*$ as

$$\frac{d}{dt} R_{Tot}^* = a_r^l T_{Tot} R - d_r^l \frac{K_r}{K_r + 1-a} R_{Tot}^* + \eta_r \quad (9)$$

$$\frac{d}{dt} B_{p, Tot}^* = a_b^l T_{Tot} B_p - d_b^l \frac{K_b}{K_b + a} B_{p, Tot}^* + \eta_b \quad (10)$$

with an activity-dependent unbinding step. To include variation around the mean, Langevin sources (η_m, η_r, η_b) have been added with magnitudes evaluated using the linear noise approximation (Text S1) [55,56]. The instantaneous output of the system is the fraction of active receptors $a(t) = a[m(t), L(t)]$ with a given by a MWC model, Eq. (13), for some external stimulus $L(t)$ (Methods) [22,23,43]. The noise statistics of the output $a(t)$ at steady state are calculated by linearizing the model and solving it as a multivariate Ornstein-Uhlenbeck process (Methods and Text S1) [57,58]. Parameter values for the analytical model (Tables S1 and S4) were taken to be consistent with those of the stochastic simulation **M1**.

Two important features can be noted from the form of Eqs. (8–10). First, Eqs. (9) and (10) emphasize that unbinding from the receptor lattice is a two-step process. Since CheR has higher affinity for the modification site as activity decreases, the overall rate of CheR unbinding the lattice and returning to the bulk decreases accordingly. Additionally, a smaller value of K_r , which denotes higher affinity of the localized enzyme for the modification site, leads to slower overall rates of unbinding. The argument for CheB-P unbinding is analogous. Second, since Eq. (8) depends only on the mean activity of the system and not on methylation or stimulus levels, the analytical model exhibits precise adaptation. This property follows from the mean field assumption or, equivalently, the assumption of fully distributive kinetics.

Using this analytical model, we next examine the mechanisms underlying the key observations made using numerical simulations and argue that: (1) large fluctuations in receptor activity are primarily due to noise in localized enzyme counts amplified by a methylation process ultrasensitive to these counts; (2) a distributive methylation scheme increases signaling noise by increasing the ultrasensitivity of this process; (3) the localized enzymes work at saturation without causing the mean activity to be ultrasensitive with respect to total enzyme expression levels. This result contrasts with the covalent modification scheme studied by Goldbeter and Koshland [12].

High levels of signaling noise arise from fluctuations in localized enzyme counts amplified by saturated methylation kinetics

The analytical model derived above predicts large fluctuations in receptor activity (Fig. 4A, black), similar to those predicted by the stochastic simulation **M1**. This level of signaling noise is significantly higher at all CheR levels than the level predicted when enzyme localization is not taken into account (Fig. 4A, gray; analytical version of model **B1** [43]). The high level of intracellular signaling noise in this system arises from three key features.

First, since the total numbers of CheR and CheB are small [52], the relative variation in the number of localized enzymes due to Poisson statistics is large. The overall rates of methylation and demethylation are therefore highly variable in time. Second, these fluctuations in localized enzyme counts occur at sufficiently slow time scales [36] to not be filtered out by the methylation process. The possibility of slow fluctuations in the number of tethered enzymes leading to increased fluctuation in receptor activity was previously noted using a model of a single MWC complex [38]. Third, the interaction between the localized enzymes and the substrate occurs at saturation. Since the binding of the localized enzymes to the receptor modification site is activity-dependent, this interaction takes the same form as the covalent modification system studied by Goldbeter and Koshland [12], as can be seen from Eq. (8). Therefore we may analyze the localized enzyme-receptor interaction in the same terms. Since a localized enzyme is confined to the tether radius, the effective local substrate concentration is high and binding to the modification site proceeds at a fast rate. Therefore, $K_r, K_b \ll 1$ and, following Goldbeter and Koshland, the steady-state output a_0 has ultrasensitive dependence on the ratio of localized CheR to CheB-P (Fig. 4B, steep curve). This steep relationship suggests that the output of the system is in general highly susceptible to changes in the ratio of localized CheR to CheB-P and, consequently, fluctuations in this ratio are the primary source of noise in the output. In the limit in which methylation is fast relative to enzyme localization, $dm/dt \sim 0$, Eq. (8) yields $a = a \left(R_{Tot}^* / B_{p, Tot}^* \right)$. In this limit, receptor activity is a function of only the ratio of the localized adaptation enzymes, corresponding to the steep curve of Fig. 4B. Likewise, the variance in receptor activity becomes $\sigma_{aa} = \left[da_0 / d \left(R_{Tot}^* / B_{p, Tot}^* \right) \right]^2 \text{var} \left(R_{Tot}^* / B_{p, Tot}^* \right)$. Therefore when the catalytic step is fast relative to enzyme localization, fluctuations in the localized enzyme ratio are amplified by exactly this steep curve. This limit case is relevant for understanding the behavior of our analytic and numerical models, in which the rates of enzyme localization are slow relative to all other rates in the system.

We may also show that fluctuations in the number of localized CheR and CheB are the dominant noise sources in the system without assuming $dm/dt \sim 0$. To illustrate this point, we use the analytical model to decompose the total variance σ_{aa} of the receptor activity into a sum of three terms, each plotted in the inset of Fig. 4B:

$$\sigma_{aa} = \sigma_{aa,r} + \sigma_{aa,b} + \sigma_{aa,m}, \quad (11)$$

fluctuations due to the number of localized CheR ($\sigma_{aa,r}$), those due to number of localized CheB-P ($\sigma_{aa,b}$), and fluctuations due to intrinsic variability in the methylation and demethylation rates ($\sigma_{aa,m}$). Each contribution $\sigma_{aa,i}$ depends linearly on the intensity of the corresponding noise source η_i in Eqs. (8–10), $\sigma_{aa,i} \propto \langle \eta_i^2 \rangle$. The magnitude of the third term $\sigma_{aa,m}$ is comparable to the total noise

predicted by models without enzyme localization. Fig. 4B (inset) shows that the first two terms on the right hand side of Eq. (11) dominate to the exclusion of the third, confirming that variability in localized CheR and CheB-P is the dominant source of the large fluctuations in receptor activity.

This same mechanism underlies the observed large fluctuations in the stochastic simulation of the model **M1**, considered previously. Fig. 4C shows mean activity a_0 versus the ratio of mean localized CheR to mean localized CheB-P obtained from simulation by varying only the total CheR count. As in the analytical model, this relationship is highly ultrasensitive. To illustrate the dependence between fluctuations in the localized enzyme ratio and fluctuations in receptor activity, the inset of Fig. 4C displays 500 s time traces of receptor activity and the ratio of localized CheR to localized CheB-P taken from simulation. The correlation between the two series is apparent and consistent with activity fluctuations arising from variability in the number of tethered enzymes.

In summary, clustering of the receptors leads to a high density of modification sites for the enzymes localized at the cluster. This results in saturated ultrasensitive kinetics of the covalent modification reactions, which strongly amplify the noise due to the slow exchange of enzymes between the cluster and the bulk.

Relation between distributive receptor modification and high levels of signaling noise

In the analytical model, large fluctuations in receptor activity result from the high affinity of localized enzymes for the modification site. Since all receptors in the analytical model are assumed to have the same activity, this affinity is entirely characterized by the small values of the constants K_r and K_b . In the numerical models, in contrast, the binding of enzymes to individual receptor dimers within MWC complexes of varying levels of activity is explicitly simulated. Consequently, the affinity of the enzymes for the modification site depends not just on the values of K_r and K_b (as derived from the binding, unbinding, and catalytic rates in the simulation), but also on the distribution of CheR and CheB within complexes of different activities. If enzymes tend to become localized within regions of the cluster for which they have low binding affinity (e.g., CheR within a highly methylated region), we expect the ultrasensitive dependence of activity on the ratio of localized enzymes (Fig. 4C) to be reduced. This effect may be thought of as increasing the effective values of K_r and K_b .

Adaptational assistance and brachiation mitigate this effect to some extent by enabling localized enzymes to sample a number of receptors during their residence time in the cluster. A higher rate of sampling indicates that a given enzyme samples a larger fraction of the cluster between subsequent methylation events and therefore corresponds to more distributive methylation kinetics. A potentially analogous situation has been studied theoretically for a MAP kinase cascade [13]. In this system, slowly diffusing enzymes tended to rebind the same substrate molecule multiple times, leading to a processive modification scheme. Faster diffusion enabled the enzymes to randomize their positions between modification events, corresponding to distributive modification. In the MAP kinase study, faster diffusion led to an ultrasensitive dependence of the output on enzyme levels. Is a similar mechanism at work in the chemoreceptor cluster?

For our numerical models, we quantified the rates at which enzymes sampled different, unique receptors within the cluster and found that this rate was between 4 and 13-fold smaller for the more processive models **M2** and **M3** than for the reference model **M1** (Table S7). Accordingly, the steady-state activity in

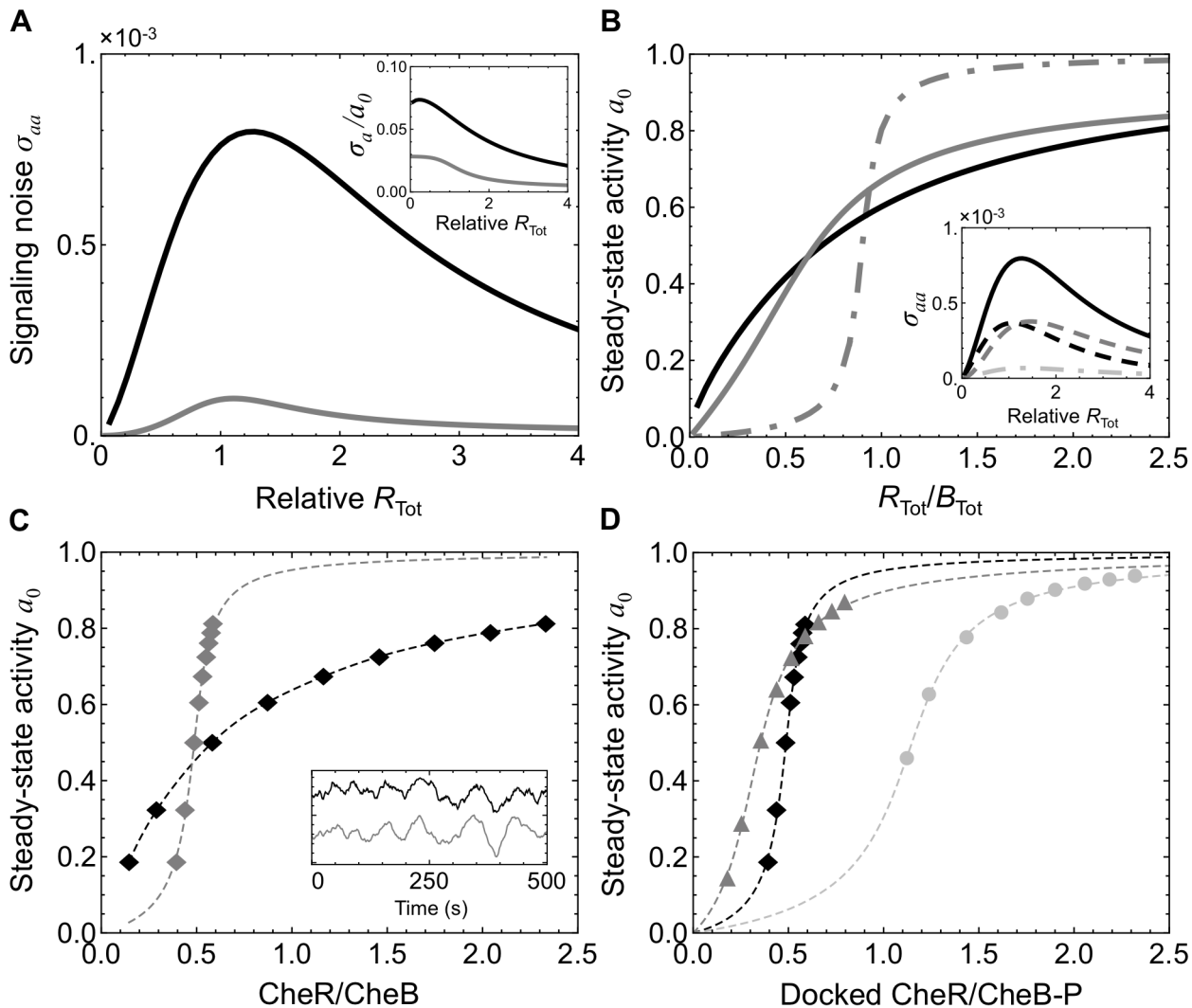


Figure 4. Large fluctuations arise from the saturated kinetics of localized enzymes. (A) Variance of receptor activity σ_{aa} at steady state is significantly larger for the analytical model with localization (black) than without localization (gray; analytical version of model **B1**) for all values of total CheR R_{Tot} . The analytical model with localization (inset, black) exhibits signaling noise with σ_{aa}/a_0 up to $\sim 7\%$ while noise in the model with no localization (analytical version of **B1**) remains at or below 3% of the mean output (inset, gray). (B) Mean receptor activity a_0 at steady state as a function of CheR to CheB ratio. When plotted as a function of the total CheR to total CheB ratio, a_0 exhibits a similar relatively robust profile for both the analytical model with localization (black) and without localization (gray; analytical version of **B1**). In contrast the mean receptor activity is ultrasensitive to the ratio of the localized CheR to localized CheB-P counts (gray, dot-dashed), $R_{Tot}^*/B_{p, Tot}^*$. (Inset) Variance in receptor activity σ_{aa} (black, solid) decomposed into components due to fluctuation in localized CheR (black, dashed), localized CheB (gray, dashed), and small intrinsic fluctuations in the methylation rates (gray, dot-dashed) as in Eq. (11). All quantities are plotted as functions of relative R_{Tot} . (C) In the stochastic simulation of **M1**, steady-state activity a_0 also has ultrasensitive dependence on the ratio of tethered CheR/CheB-P (gray), despite the weak dependence on total CheR/CheB (black). (Inset) 500 s simulation trace of instantaneous mean receptor activity $a(t)$ (black) and instantaneous localized CheR/CheB-P (gray), smoothed with a 30 s sliding window average. (D) Comparison of the dependence of a_0 on localized CheR/CheB-P for the simulated models **M1** (black), **M2** (light gray), and **M3** (dark gray) from Fig. 2. This dependence is significantly weaker for the more processive models.

doi:10.1371/journal.pcbi.1003230.g004

the more processive models **M2** and **M3** is also less dependent on the ratio of localized CheR to CheB-P than in **M1** (Fig. 4D). Since this relationship effectively amplifies fluctuations in the ratio of localized enzymes, this decreased steepness leads to lower signaling noise levels in these more processive models, as seen previously (Fig. 2C). For further details regarding the comparison between simulations and the analytical model, see Supporting Text S1. We conclude that a distributive methylation scheme leads to higher signaling noise levels by increasing the overall affinity of the localized enzymes for the modification site substrate.

Localized enzymes may work at saturation without compromising robustness to cell-to-cell variability in total enzyme expression levels

The mean steady-state activity for the analytical model with enzyme localization is plotted in Fig. 4B as a function of the ratio of both localized and total (across the entire cell) adaptation enzymes, $R_{Tot}^*/B_{p, Tot}^*$ and R_{Tot}/B_{Tot} . While the activity is highly ultrasensitive with respect to the localized enzyme ratio, its sensitivity to the total enzyme ratio is significantly less and comparable to the model **B1**. Therefore, the mean steady-state

activity of the system a_0 is robust to changes in the total CheR to CheB ratio caused by noisy gene expression. This result is somewhat surprising because in the classic covalent modification system studied by Goldbeter and Koshland [12], saturated enzyme-substrate interactions always lead to a steady-state activity that is ultrasensitive to the total CheR to CheB ratio.

In Eq. (8), which we may analyze in the same manner as the Goldbeter-Koshland system, the sensitivity of the steady-state activity a_0 with respect to the ratio of localized CheR to CheB is determined solely by the constants (K_r, K_b) that characterize the probability that a localized enzyme will be bound to a modification site. Small values of these constants lead to saturated kinetics and ultrasensitivity of the steady-state activity to the ratio of *localized* CheR to CheB. Our model differs from the Goldbeter-Koshland system, however, in that in our model these constants only partially determine the sensitivity of a_0 to the ratio of *total* CheR to CheB. The sensitivity of the system to the total enzyme ratio is also determined by the rates at which cytoplasmic enzymes localize to the cluster and at which localized enzymes return to the bulk. Since the rates (a_r^t, a_b^t) at which enzymes localize to the cluster are slow [36], the effective affinities of the enzymes for the modification sites are reduced even though the affinities of enzymes already localized at the cluster are high.

The steady-state solutions to Eqs. (8–10) quantify how the mean steady-state activity depends on the total enzyme counts R_{Tot} and B_{Tot} . Solving Eqs. (9) and (10) for the localized enzyme counts R_{Tot}^* and $B_{p, Tot}^*$ and inserting the results into Eq. (8), we obtain

$$\frac{dm}{dt} = \frac{k_r R_{Tot}(1-a)}{K_r(1+d_r^t/a_r^t T_{Tot})+1-a} - \frac{k_b B_{Tot}a}{K_b[1+d_b^t/a_b^t T_{Tot}(1+d_p/a_p T_{Tot}a)]+a} = 0. \quad (12)$$

Eq. (12) is also of the Goldbeter-Koshland form which indicates that the steepness of the steady-state activity as a function of the total CheR to CheB ratio is determined by the effective inverse affinities $K'_r = K_r(1+d_r^t/a_r^t T_{Tot})$ and $K'_b(a) = K_b[1+d_b^t/a_b^t T_{Tot}(1+d_p/a_p T_{Tot}a)]$. Values of $K'_{r,b} \ll 1$ lead to ultrasensitivity of the steady-state activity with respect to the ratio R_{Tot}/B_{Tot} . For the steady-state activity to be considered robust, we require $K'_{r,b} \sim 1$. From this condition, we can see that the steady-state a_0 can be robust even if the affinity of the localized enzymes for the modification site is extremely high, $(K_r, K_b) \ll 1$. This will be the case if the rates $a'_{r,b}$ of enzymes in the bulk to reach the cluster and bind the tether are sufficiently small relative to the unbinding rates $d'_{r,b}$, effectively compensating for the small (K_r, K_b) and leading to $K'_{r,b} \sim K_{r,b} d'_{r,b}/a'_{r,b} T_{Tot} \sim 1$.

To discuss the robustness of the bacterial chemotaxis system, we note three key considerations. First, we estimate that $K_r, K_b \ll 1$ due to the fast rate of the highly localized enzymes binding the modification site (Text S1). Second, we note that the CheB-P feedback loop is not by itself sufficient to make the steady-state robust to the total enzyme ratio. While the term due to the feedback loop in $K'_b, 1+d_p/a_p T_{Tot}a$, is greater than 1 and therefore confers some degree of robustness, for typical values of activity, $a \sim 0.2$ or greater, the term is only of order 1 and therefore not sufficient to compensate for small K_b . Robustness therefore likely arises from the slow kinetics of tether binding. The final consideration is that measurements [36] indicate that the number

of cytoplasmic and localized enzymes are comparable and therefore that the forward and reverse rates of Eqs. (9) and (10) are roughly equal. This condition not only leads to comparable numbers of localized and cytoplasmic enzymes, but also indicates that the rates of tether binding and unbinding fall in the regime in which the steady-state activity is robust to the total number of enzymes. Specifically, for CheR, requiring the forward and backward rates of Eq. (9) to be comparable yields $a_r^t T_{Tot} - d_r^t K_r / (K_r + 1 - a) - d_b^t K_r / (1 - a)$, leading to $K_r d_r^t / a_r^t T_{Tot} \sim K'_r - 1$ for typical values of a (0.3–0.5) [43]. The argument for CheB is analogous. Satisfying this constraint therefore leads not only to both comparable numbers of localized and cytoplasmic enzymes, but also to a steady-state activity that is robust to the total enzyme ratio. In this manner, the steady-state of the bacterial chemotaxis system can remain robust even when the localized enzymes operate at saturation.

Discussion

Chemotactic bacteria are able to navigate chemical gradients with strengths ranging over five orders of magnitude [19]. This remarkable capability results from the capacity of the system to amplify small input signals while adapting to a wide range of concentrations of persistent stimulus. The cooperative receptor-receptor interactions that amplify input signals are facilitated by the formation of large receptor clusters, structures that are strongly conserved across bacterial species [5]. Adaptation to stimulus requires the efficient recruitment of cytoplasmic enzymes to these clusters, which is achieved through the presence of a high-affinity enzyme-tethering site on most receptors. These tethers, together with the dense structure of the receptor lattice, give rise to assistance neighborhoods [27] and possibly enzyme brachiation [37]. These features increase the distributivity of methylation, decreasing the likelihood that enzymes become localized in neighborhoods within which they have low binding affinity and therefore act inefficiently.

Building on previous work that showed assistance neighborhoods were necessary for precise adaptation in a single strongly coupled signaling complex [28,38], we found that assistance neighborhoods and enzyme brachiation contributed to precise adaptation to stimulus. We further linked distributive methylation to the presence of signaling noise in the output and showed how high signaling noise may coexist with a mean level of receptor activity that is robust to changes in the ratio of the adaptation enzymes. This ratio is not exactly conserved across populations. Consequently, if the mean activity were not sufficiently robust, the ultrasensitivity of the flagellar motor [59,60] would lead to a significant fraction of nonfunctional cells permanently in the running or tumbling state. This robustness to the ratio of adaptation enzymes occurs even though the localized enzymes work in the saturated regime. This scheme is not possible for the simpler covalent modification system studied by Goldbeter and Koshland, in which saturated enzyme kinetics always corresponds to ultrasensitivity to the enzyme ratio.

The mechanism described here is not necessarily restricted solely to the bacterial chemotaxis system. The analytical model presented in this study describes generally an extension of the Goldbeter-Koshland [12] motif in which enzymes transition between active and inactive states, whether by localization to the substrate prior to modification, as in the bacterial chemotaxis model, or by chemical activation of the enzyme. This simplified model captures the essential features underlying large fluctuations: slow enzyme activation relative to the modification rate, saturated

kinetics between the activated enzyme and the substrate, and distributive modification. While the kinetics of activated enzyme and substrate may be saturated, the robustness of the system to the overall expression levels of the enzymes may be preserved if the enzyme activation (localization) rate is sufficiently small relative to the deactivation (delocalization) rate. The effects of enzyme localization and the relationship between rapid enzyme rebinding and processivity have been considered in studies of MAP kinase cascades. A recent study of the mating response in yeast [61] discusses a mechanism in which the kinase Fus3 and phosphatase Ptc1 bind a docking site on the substrate Ste5 prior to modification. Since the docked enzymes operate at saturation, the system is ultrasensitive to changes in the number of recruited enzymes, similar to the chemoreceptor-enzyme system discussed in this work. Unlike the chemotaxis system, however, yeast exploits these saturated kinetics to produce a switch-like response in the steady state. The theoretical work of Takahashi *et al.* [13] also considers the MAP kinase system, using it as a model to explore the role of enzyme diffusion in determining whether substrate modification is processive or distributive. The authors conclude that slow diffusion, which causes the enzyme to bind and phosphorylate the same substrate molecule repeatedly, can effectively convert a distributive mechanism into a processive one, reducing the sensitivity of the system. The same effect figures prominently in our model of the bacterial chemotaxis system but in the opposite regime, in which the brachiation process serves to randomize enzyme positions between methylation events.

Future studies of the bacterial chemotaxis system may further clarify the role of enzyme brachiation in adaptation. Different configurations of clustered receptors from that considered here, such as less dense clusters that have been shown to reduce cooperativity [62], or larger numbers of significantly smaller clusters [63], could hinder the ability of localized enzymes to visit a large number of unique receptors. In these cases our results suggest that signaling noise would be reduced. Interestingly, brachiation may be particularly important when considering cluster structure within local adaptation models [64]. In these models, receptors of different types respond specifically to different stimuli. Consequently, successful adaptation may depend on the ability of the adaptation enzymes to localize efficiently to responsive receptors. Brachiation may be critical for such efficient localization, particularly when considering the adaptation of low abundance receptors to their specific stimuli.

While many systems benefit from minimizing signaling noise, studies of bacterial chemotaxis have shown that noise may increase the performance of the system in sparse environments while introducing only minimal deleterious effects. In empty environments, signaling noise may lead to faster cellular exploration to locate nutrient sources more efficiently [32,33,39]. Signaling noise has also been shown theoretically to increase tracking performance in shallow gradients [32,33,35]. These results are consistent with a picture of the chemotaxis system being not purely a signal transduction system, for which minimizing noise would typically be desirable, but also a feedback system in which the output controls the sampling of the input.

Methods

Receptor activation

Since changes in receptor activity are effectively instantaneous relative to the slow methylation kinetics, activation of the receptor clusters is described by an equilibrium MWC model [22,23]. Clusters in the model are composed of $N=6$ Tar homodimers. The free energy difference between the active and inactive states of

the cluster is decreased by ε_1 per methylation level and increased by $N \log[(1+L/K)/(1+L/K^\varepsilon)]$ in the presence of methyl-aspartate attractant L . Then the fraction of active clusters is given by

$$a(m,L) = \frac{1}{1 + \exp(\varepsilon_0 - \varepsilon_1 m) \left(\frac{1+L/K}{1+L/K^\varepsilon} \right)^N} \quad (13)$$

with m the methylation level. Parameter values were taken from fits to dose response measurements [43] and reproduced in Table S1. In the stochastic simulation, m is taken to be the methylation level of a single MWC signaling unit and $a(m, L)$ is used to calculate the activity of each MWC unit individually. In the analytical model, following Shimizu *et al.* [43], m is the average methylation level per receptor cluster and $a(m, L)$ is taken to be the average activity of all receptors in the system.

Signaling properties

We analyze the signaling properties of the model Eqs. (8–10) by performing a perturbation analysis around the steady state. Small displacements in the numbers of chemical species \mathbf{x} evolve according to the linear system of Itô stochastic differential equations

$$d\mathbf{x}(t) = A\mathbf{x}(t)dt + Bd\mathbf{W}(t) \quad (14)$$

in which A is the Jacobian matrix of the system, B is the diffusion matrix, and $\mathbf{W}(t)$ is the multidimensional Wiener process. By the linear noise approximation, $B^T B = S \text{diag}(\mathbf{v}) S^T$ with S the stoichiometry matrix and \mathbf{v} the propensity vector [55,56]. The system in Eq. (14) is a multivariate Ornstein-Uhlenbeck process [57]. A has eigenvalues with negative real components, indicating the system relaxes to steady state after perturbation. The steady-state variance in the output of the system is obtained by solving the Lyapunov equation

$$A\sigma + \sigma A^T + B^T B = 0 \quad (15)$$

for the covariance matrix σ . Additional details of the noise calculation are presented in the Supporting Text S1.

Supporting Information

Figure S1 Structuring the chemoreceptor lattice in NFsim. (A) A MWC signaling complex consisting of two trimers of dimers (left) is specified by enumerating bonds (right, blue) between a dimer and all of its neighbors within the complex. (B) The hexagonal lattice is then structured by enumerating bonds between a given dimer and all of its neighbors in other signaling complexes (red). The pictured lattice consists of 21 MWC complexes. All interior dimers have six neighbors. The basic unit of the lattice is the hexagon consisting of three signaling complexes. We model lattices of equal length and width, as specified in terms of this basic hexagonal unit. (TIFF)

Figure S2 Response of the numerical model **M1** to time-varying exponential ramps of chemoattractant. We presented the simulated cells with exponential ramps of methyl-aspartate (light gray, plotted in arbitrary units) of rate r (shown in each panel) and averaged the response in receptor activity over ten trials (dark gray). For each ramp, receptor activity approached a steady-state value during stimulus, determined by exponential fits (black) to $a(t)$ and plotted in Fig. 2A of the main text. Following a recent

experiment [43], the methyl-aspartate concentration ranged between 0.084 and 0.62 mM.

(TIFF)

Figure S3 Fluctuations in the analytical model with no enzyme localization. The noise level within a narrow range of CheR values increases as the dependence of the steady-state activity on CheR count becomes steeper. (A) Steady state activity a_0 as a function of normalized CheR count for the parameters used in Fig. 4 (gray) and with Michaelis-Menten constants K_r and K_b reduced by a factor of 10 (black). The latter curve exhibits an extreme dependence on variations in CheR count. (B) Variance σ_{aa} and relative noise σ_a/a_0 (inset) in activity at the steady state as a function of normalized CheR count for original (gray) and reduced K_r and K_b (black). Reducing K_r and K_b increases the relative noise level to nearly 5%.

(TIFF)

Figure S4 Increasing the distributivity of methylation in the detailed analytical model (Text S1) increases noise and the affinity of localized enzymes for the receptor substrate. (A) Variance σ_{aa} in overall activity as a function of total CheR count for fully processive methylation, $\beta = 0$ (gray), and more distributive methylation, $\beta = 20 \text{ s}^{-1}$ (black) (B) The steady-state activity a_0 as a function of total CheR is similar for both $\beta = 0$ (gray) and $\beta = 20 \text{ s}^{-1}$ (black). (C) Steady-state activity a_0 versus localized CheR/CheB-P, $R_{Tot}^*/B_{p,Tot}^*$ is much steeper in the more distributive model with $\beta = 20 \text{ s}^{-1}$ (black) than $\beta = 0$ (gray).

(TIFF)

Figure S5 Estimated distribution of overall chemotaxis protein expression levels in a wild-type population relative to the most common expression level. We sampled representative cells (points) from a population in which the ratio CheR/CheB/chemoreceptors is maintained while the overall expression level follows a log-normal distribution. Signaling noise levels for these representative cells are shown in Fig. 3A of the main text.

(TIFF)

Figure S6 Mean fraction of “inert” CheB-P tethered within fully demethylated assistance neighborhoods (for models **M1**, black, and **M3**, light gray) or with fully demethylated receptor dimers (**M2**, dark gray) versus total CheR. These enzymes may bind the modification sites of receptors but will be unable to demethylate once bound. These enzymes are unable to affect the activity of the receptor cluster and are therefore not counted when calculating the ratio of localized CheR to CheB-P for Fig. 4. Since very few receptors are fully methylated, the number of inert, localized CheR is negligible (<1) for all models. This situation arises because MWC signaling complexes are highly active even at low methylation levels: in the absence of stimulus, $a = 0.5$ for $m = 6$ (out of 48) and $a \sim$ for $m = 14$. Consequently, many receptor dimers are fully demethylated even for cases in which the average

receptor activity is high. In contrast, full methylated dimers are rare.

(TIFF)

Figure S7 Average methylation level per MWC complex as a function of time for numerical models **M1** (black), **M2** (light gray), and **M3** (dark gray) during the simulations shown in Fig. 2B (lower panel) of the main text. A step stimulus of 1 mM MeAsp was presented at 200 s. The most distributive model **M1** displays the highest methylation rate during the adaptation process.

(TIFF)

Table S1 Parameter names and values common to all models. (PDF)

Table S2 Parameter values for stochastic simulation of model **M1** with enzyme localization. Rates are designated as in Fig. 1B with an r or b subscript to denote rates of CheR and CheB reactions. (PDF)

Table S3 Parameter values for stochastic simulation of the model **B1** with no enzyme localization. (PDF)

Table S4 Parameter values for mean-field analytical model with enzyme localization. All values are derived from values of corresponding parameters in the numerical model **M1** (Table S2). (PDF)

Table S5 Parameter values for analytical version of model **B1** with no enzyme localization. (PDF)

Table S6 Changes in parameter values for the derived models **M2**, **M3**, and **B2**. (PDF)

Table S7 Number of unique dimers visited by localized enzymes per second for the numerical models. Higher rates indicate more distributive methylation. (PDF)

Text S1 Additional details regarding model derivations, implementations, and analysis. (PDF)

Acknowledgments

The authors thank Tom Shimizu, Yann Dufour, and Nicholas Frankel for helpful discussions and comments on the manuscript.

Author Contributions

Analyzed the data: WP TE. Contributed reagents/materials/analysis tools: MWS. Wrote the paper: WP TE. Conceived and designed the research: WP TE. Performed the research: WP. Designed and performed the biochemical simulations: WP MWS. Designed the analytical models: WP.

References

- Bourret RB, Borkovich KA, Simon MI (1991) Signal transduction pathways involving protein phosphorylation in prokaryotes. Annual review of biochemistry 60: 401–441.
- Lauffenburger DA, Linderman JJ (1993) Receptors models for binding, trafficking, and signaling. New York: Oxford University Press. 365 p.
- Alley MR, Maddock JR, Shapiro L (1992) Polar localization of a bacterial chemoreceptor. Genes Dev 6: 825–836.
- Briegel A, Li XX, Bilwes AM, Hughes KT, Jensen GJ, et al. (2012) Bacterial chemoreceptor arrays are hexagonally packed trimers of receptor dimers networked by rings of kinase and coupling proteins. P Natl Acad Sci USA 109: 3766–3771.
- Briegel A, Ortega DR, Tocheva EI, Wuichet K, Li Z, et al. (2009) Universal architecture of bacterial chemoreceptor arrays. P Natl Acad Sci USA 106: 17181–17186.
- Liu J, Hu B, Morado DR, Jani S, Manson MD, et al. (2012) Molecular architecture of chemoreceptor arrays revealed by cryoelectron tomography of Escherichia coli minicells. P Natl Acad Sci USA 109: E1481–E1488.
- Abulrob A, Lu Z, Baumann E, Vobornik D, Taylor R, et al. (2010) Nanoscale imaging of epidermal growth factor receptor clustering: effects of inhibitors. The Journal of biological chemistry 285: 3145–3156.
- Bunnell SC, Hong DI, Kardon JR, Yamazaki T, McGlade CJ, et al. (2002) T cell receptor ligation induces the formation of dynamically regulated signaling assemblies. The Journal of cell biology 158: 1263–1275.
- Bray D, Levin MD, Morton-Firth CJ (1998) Receptor clustering as a cellular mechanism to control sensitivity. Nature 393: 85–88.
- Duke TA, Bray D (1999) Heightened sensitivity of a lattice of membrane receptors. Proc Natl Acad Sci U S A 96: 10104–10108.

11. Bialek W, Setayeshgar S (2005) Physical limits to biochemical signaling. *P Natl Acad Sci USA* 102: 10040–10045.
12. Goldbeter A, Koshland DE (1981) An Amplified Sensitivity Arising from Covalent Modification in Biological-Systems. *P Natl Acad Sci-Biol* 78: 6840–6844.
13. Takahashi K, Tanase-Nicola S, ten Wolde PR (2010) Spatio-temporal correlations can drastically change the response of a MAPK pathway. *P Natl Acad Sci USA* 107: 2473–2478.
14. Mugler A, Bailey AG, Takahashi K, ten Wolde PR (2012) Membrane Clustering and the Role of Rebinding in Biochemical Signaling. *Biophys J* 102: 1069–1078.
15. Benichou O, Chevalier C, Klafter J, Meyer B, Voituriez R (2010) Geometry-controlled kinetics. *Nat Chem* 2: 472–477.
16. Berg HC (2000) Motile Behavior of Bacteria. *Physics Today* 53: 24–29.
17. Wadhams GH, Armitage JP (2004) Making sense of it all: Bacterial chemotaxis. *Nat Rev Mol Cell Bio* 5: 1024–1037.
18. Sourjik V, Wingreen NS (2012) Responding to chemical gradients: bacterial chemotaxis. *Curr Opin Cell Biol* 24: 262–268.
19. Mesibov R, Adler J (1972) Chemotaxis toward Amino-Acids in *Escherichia-Coli*. *J Bacteriol* 112: 315–326.
20. Sourjik V, Berg HC (2002) Receptor sensitivity in bacterial chemotaxis. *P Natl Acad Sci USA* 99: 123–127.
21. Sourjik V, Berg HC (2004) Functional interactions between receptors in bacterial chemotaxis. *Nature* 428: 437–441.
22. Mello BA, Tu YH (2005) An allosteric model for heterogeneous receptor complexes: Understanding bacterial chemotaxis responses to multiple stimuli. *P Natl Acad Sci USA* 102: 17354–17359.
23. Keymer JE, Endres RG, Skoge M, Meir Y, Wingreen NS (2006) Chemosensing in *Escherichia coli*: Two regimes of two-state receptors. *P Natl Acad Sci USA* 103: 1786–1791.
24. Yi TM, Huang Y, Simon MI, Doyle J (2000) Robust perfect adaptation in bacterial chemotaxis through integral feedback control. *P Natl Acad Sci USA* 97: 4649–4653.
25. Barkai N, Leibler S (1997) Robustness in simple biochemical networks. *Nature* 387: 913–917.
26. Alon U, Surette MG, Barkai N, Leibler S (1999) Robustness in bacterial chemotaxis. *Nature* 397: 168–171.
27. Li MS, Hazelbauer GL (2005) Adaptational assistance in clusters of bacterial chemoreceptors. *Mol Microbiol* 56: 1617–1626.
28. Endres RG, Wingreen NS (2006) Precise adaptation in bacterial chemotaxis through “assistance neighborhoods”. *P Natl Acad Sci USA* 103: 13040–13044.
29. Andrews BW, Yi TM, Iglesias PA (2006) Optimal noise filtering in the chemotactic response of *Escherichia coli*. *Plos Comput Biol* 2: e154.
30. Emonet T, Cluzel P (2008) Relationship between cellular response and behavioral variability in bacterial chemotaxis. *P Natl Acad Sci USA* 105: 3304–3309.
31. Vladimirov N, Lovdok L, Lebedez D, Sourjik V (2008) Dependence of bacterial chemotaxis on gradient shape and adaptation rate. *Plos Comput Biol* 4: e1000242.
32. Matthaus F, Jagodic M, Dobnikar J (2009) *E. coli* Superdiffusion and Chemotaxis-Search Strategy, Precision, and Motility. *Biophys J* 97: 946–957.
33. Sneddon MW, Pontius W, Emonet T (2012) Stochastic coordination of multiple actuators reduces latency and improves chemotactic response in bacteria. *P Natl Acad Sci USA* 109: 805–810.
34. Zhu X, Si G, Deng N, Ouyang Q, Wu T, et al. (2012) Frequency-dependent *Escherichia coli* chemotaxis behavior. *Phys Rev Lett* 108: 128101.
35. Flores M, Shimizu TS, ten Wolde PR, Tostevin F (2012) Signaling noise enhances chemotactic drift of *E. coli*. *Phys Rev Lett* 109: 148101.
36. Schulmeister S, Ruttorf M, Thiem S, Kentner D, Lebedez D, et al. (2008) Protein exchange dynamics at chemoreceptor clusters in *Escherichia coli*. *P Natl Acad Sci USA* 105: 6403–6408.
37. Levin MD, Shimizu TS, Bray D (2002) Binding and diffusion of CheR molecules within a cluster of membrane receptors. *Biophys J* 82: 1809–1817.
38. Hansen CH, Endres RG, Wingreen NS (2008) Chemotaxis in *Escherichia coli*: a molecular model for robust precise adaptation. *Plos Comput Biol* 4: e1.
39. Korobkova E, Emonet T, Vilar JMG, Shimizu TS, Cluzel P (2004) From molecular noise to behavioural variability in a single bacterium. *Nature* 428: 574–578.
40. Park H, Pontius W, Guet CC, Marko JF, Emonet T, et al. (2010) Interdependence of behavioural variability and response to small stimuli in bacteria. *Nature* 468: 819–823.
41. Park H, Oikonomou P, Guet CC, Cluzel P (2011) Noise Underlies Switching Behavior of the Bacterial Flagellum. *Biophys J* 101: 2336–2340.
42. Tu YH, Grinstein G (2005) How white noise generates power-law switching in bacterial flagellar motors. *Phys Rev Lett* 94: 208101.
43. Shimizu TS, Tu YH, Berg HC (2010) A modular gradient-sensing network for chemotaxis in *Escherichia coli* revealed by responses to time-varying stimuli. *Mol Syst Biol* 6: 382.
44. Kollmann M, Lovdok L, Bartholome K, Timmer J, Sourjik V (2005) Design principles of a bacterial signalling network. *Nature* 438: 504–507.
45. Sneddon MW, Faeder JR, Emonet T (2011) Efficient modeling, simulation and coarse-graining of biological complexity with NFsim. *Nat Methods* 8: 177–183.
46. Windisch B, Bray D, Duke T (2006) Balls and chains - A mesoscopic approach to tethered protein domains. *Biophys J* 91: 2383–2392.
47. Kentner D, Sourjik V (2009) Dynamic map of protein interactions in the *Escherichia coli* chemotaxis pathway. *Mol Syst Biol* 5: 238.
48. Ishihara A, Segall JE, Block SM, Berg HC (1983) Coordination of Flagella on Filamentous Cells of *Escherichia-Coli*. *J Bacteriol* 155: 228–237.
49. Korobkova EA, Emonet T, Park H, Cluzel P (2006) Hidden stochastic nature of a single bacterial motor. *Phys Rev Lett* 96: 058105.
50. Min TL, Mears PJ, Chubiz LM, Rao CV, Golding I, et al. (2009) High-resolution, long-term characterization of bacterial motility using optical tweezers. *Nat Methods* 6: 831–835.
51. Lovdok L, Kollmann M, Sourjik V (2007) Co-expression of signaling proteins improves robustness of the bacterial chemotaxis pathway. *J Biotechnol* 129: 173–180.
52. Li MS, Hazelbauer GL (2004) Cellular stoichiometry of the components of the chemotaxis signaling complex. *J Bacteriol* 186: 3687–3694.
53. Mello BA, Tu Y (2003) Perfect and near-perfect adaptation in a model of bacterial chemotaxis. *Biophys J* 84: 2943–2956.
54. Rao CV, Kirby JR, Arkin AP (2004) Design and diversity in bacterial chemotaxis: A comparative study in *Escherichia coli* and *Bacillus subtilis*. *Plos Biol* 2: 239–252.
55. Gillespie DT (2000) The chemical Langevin equation. *J Chem Phys* 113: 297–306.
56. Elf J, Ehrenberg M (2003) Fast evaluation of fluctuations in biochemical networks with the linear noise approximation. *Genome Res* 13: 2475–2484.
57. Gardiner CW (2004) Handbook of stochastic methods for physics, chemistry, and the natural sciences. Berlin; New York: Springer-Verlag. 415 p.
58. Kampen NGv (2007) Stochastic processes in physics and chemistry. Amsterdam; New York: Elsevier. 463 p.
59. Cluzel P, Surette M, Leibler S (2000) An ultrasensitive bacterial motor revealed by monitoring signaling proteins in single cells. *Science* 287: 1652–1655.
60. Yuan J, Berg HC (2013) Ultrasensitivity of an Adaptive Bacterial Motor. *Journal of molecular biology* 425: 1760–4 doi:10.1016/j.jmb.2013.02.016.
61. Malleshaiah MK, Shahrezaei V, Swain PS, Michnick SW (2010) The scaffold protein Ste5 directly controls a switch-like mating decision in yeast. *Nature* 465: 101–105.
62. Khursigara CM, Lan G, Neumann S, Wu X, Ravindran S, et al. (2011) Lateral density of receptor arrays in the membrane plane influences sensitivity of the *E. coli* chemotaxis response. *Embo J* 30: 1719–1729.
63. Thiem S, Kentner D, Sourjik V (2007) Positioning of chemosensory clusters in *E. coli* and its relation to cell division. *Embo J* 26: 1615–1623.
64. Lan GH, Schulmeister S, Sourjik V, Tu YH (2011) Adapt locally and act globally: strategy to maintain high chemoreceptor sensitivity in complex environments. *Mol Syst Biol* 7: 475.